AFRL-PR-WP-TP-2006-241

ASSESSING CONVERGENCE IN PREDICTIONS OF PERIODIC-UNSTEADY FLOWFIELDS

J.P. Clark
E.A. Grover

JUNE 2006

Approved for public release; distribution is unlimited.

STINFO COPY

PROPULSION DIRECTORATE
AIR FORCE MATERIEL COMMAND
AIR FORCE RESEARCH LABORATORY
WRIGHT-PATTERSON AIR FORCE BASE, OH 45433-7251

REPORT DOCUMENTATION PAGE

Form Approved
OMB No. 0704-0188

1. REPORT DATE *(DD-MM-YY)*	2. REPORT TYPE	3. DATES COVERED *(From - To)*
June 2006	Conference Paper Postprint	10/01/2005 – 05/01/2006

4. TITLE AND SUBTITLE
ASSESSING CONVERGENCE IN PREDICTIONS OF PERIODIC-UNSTEADY FLOWFIELDS

5a. CONTRACT NUMBER
In-house

5b. GRANT NUMBER

5c. PROGRAM ELEMENT NUMBER
62203F

6. AUTHOR(S)
J.P. Clark (AFRL/PRTT)
E.A. Grover (United Technologies Pratt & Whitney)

5d. PROJECT NUMBER
3066

5e. TASK NUMBER
06

5f. WORK UNIT NUMBER
W8

7. PERFORMING ORGANIZATION NAME(S) AND ADDRESS(ES)

Turbine Branch (AFRL/PRTT)
Turbine Engine Division
Propulsion Directorate
Air Force Research Laboratory, Air Force Materiel Command
Wright-Patterson Air Force Base, OH 45433-7251

Turbine Aerodynamics
United Technologies Pratt & Whitney
400 Main Street, M/S 169-29
East Harford, CT 06108

8. PERFORMING ORGANIZATION REPORT NUMBER
AFRL-PR-WP-TP-2006-241

9. SPONSORING/MONITORING AGENCY NAME(S) AND ADDRESS(ES)

Propulsion Directorate
Air Force Research Laboratory
Air Force Materiel Command
Wright-Patterson AFB, OH 45433-7251

10. SPONSORING/MONITORING AGENCY ACRONYM(S)
AFRL-PR-WP

11. SPONSORING/MONITORING AGENCY REPORT NUMBER(S)
AFRL-PR-WP-TP-2006-241

12. DISTRIBUTION/AVAILABILITY STATEMENT
Approved for public release; distribution is unlimited.

13. SUPPLEMENTARY NOTES
Conference paper postprint published in the Proceedings of GT2006, ASME TURBO EXPO 2006: Power for Land, Sea and Air, published by ASME. PAO case number: AFMC 05-417; Date cleared: 20 Oct 2005. Paper contains color.

14. ABSTRACT
Here we report on a method developed to determine the level of convergence in a predicted flowfield that is characterized by periodic-unsteadiness. The method relies on fundamental concepts from digital signal processing including the discrete Fourier transform, cross-correlation, and Parseval's theorem. Often in predictions of vane-blade interaction in turbomachines, the period of the unsteady fluctuations is expected. In this method, the development of time-mean quantities, Fourier components (both magnitude and phase), cross-correlations, and integrated signal power are tracked at locations of interest from one period to the next as the solution progresses. Each of these separate quantities yields some relative measure of convergence that is subsequently processed to form a fuzzy set. Thus the overall level of convergence in the solution is given by the intersection of these sets. It is shown that the method yields a robust determination of convergence. In addition, the method is useful for the detection of inherent unsteadiness in the flowfield, and as such it can be used to prevent design escapes.

15. SUBJECT TERMS
Turbomachinery, Convergence, Vane-Blade Interaction, Inherent Unsteadiness, Vortex Shedding, Unsteady Flows

16. SECURITY CLASSIFICATION OF:			17. LIMITATION OF ABSTRACT:	18. NUMBER OF PAGES	19a. NAME OF RESPONSIBLE PERSON (Monitor)
a. REPORT	b. ABSTRACT	c. THIS PAGE			John P. Clark
Unclassified	Unclassified	Unclassified	SAR	18	19b. TELEPHONE NUMBER *(Include Area Code)* N/A

Standard Form 298 (Rev. 8-98)
Prescribed by ANSI Std. Z39-18

Proceedings of GT2006
ASME TURBO EXPO 2006: Power for Land, Sea and Air
May 8-11, 2006, Barcelona, Spain

GT2006-90735

ASSESSING CONVERGENCE IN PREDICTIONS OF PERIODIC-UNSTEADY FLOWFIELDS

J. P. Clark
Turbine Branch, Turbine Engine Division
Propulsion Directorate, Air Force Research Laboratory
Building 18, Room 136D,
1950 5th St., WPAFB, OH 45433
john.clark3@wpafb.af.mil

E. A. Grover
Turbine Aerodynamics
United Technologies Pratt & Whitney
400 Main St., M/S 169-29
East Hartford, CT 06108
eric.grover@pw.utc.com

ABSTRACT

Predictions of time-resolved flowfields are now commonplace within the gas-turbine industry, and the results of such simulations are often used to make design decisions during the development of new products. Hence it is necessary for design engineers to have a robust method to determine the level of convergence in design predictions. Here we report on a method developed to determine the level of convergence in a predicted flowfield that is characterized by periodic-unsteadiness. The method relies on fundamental concepts from digital signal processing including the discrete Fourier transform, cross-correlation, and Parseval's theorem. Often in predictions of vane-blade interaction in turbomachines, the period of the unsteady fluctuations is expected. In this method, the development of time-mean quantities, Fourier components (both magnitude and phase), cross-correlations, and integrated signal power are tracked at locations of interest from one period to the next as the solution progresses. Each of these separate quantities yields some relative measure of convergence that is subsequently processed to form a fuzzy set. Thus the overall level of convergence in the solution is given by the intersection of these sets. Examples of the application of this technique to several predictions of unsteady flows from two separate solvers are given. These include a prediction of hot-streak migration as well as more typical cases. It is shown that the method yields a robust determination of convergence. Also, the results of the technique can guide further analysis and/or post-processing of the flowfield. Finally, the method is useful for the detection of inherent unsteadiness in the flowfield, and as such it can be used to prevent design escapes.

NOMENCLATURE

Latin

A	DFT magnitude
CCF	Cross-correlation coefficient
DFT	Discrete Fourier Transform
E	Engine order = frequency / (rpm / 60)
f	Membership grade in a fuzzy set
k	Integer multiple of sampling frequency
L	Number of lags
M	Mach number
N	Number of samples per periodic cycle
n	Integer multiple of sampling interval
P	Fourier component of static pressure signal
Pt	Total pressure (M Pa)
p	Static pressure (M Pa)
PSD	Power spectral density
Re	Reynolds number based on axial chord
Tt	Total temperature (K)

Greek

Δf	Spectral resolution (Hz) of a signal = 1 / (N Δt)
Δt	Sampling rate, temporal resolution of a signal (s)
Φ	DFT phase angle (radians, degrees)
ω	Circular frequency (radians / s)

Subscripts / Superscript

A	Fuzzy set for convergence of DFT amplitude
C	Fuzzy set for overall convergence
M	Fuzzy set for time-mean convergence
P	Fuzzy set for fraction of overall signal power
S	Fuzzy set for convergence of overall signal shape
Φ	Fuzzy set for convergence of DFT phase angle
'	Fluctuating component

INTRODUCTION

As the state-of-the-art for CFD calculations in the gas turbine industry has progressed from single-row potential flow calculations to time-resolved, multi-stage unsteady Navier-Stokes simulations, the fidelity of flowfield predictions has increased accordingly. The increased predictive capability of the codes have allowed for better turbomachinery designs and improved understanding of the physical mechanisms that are prevalent in turbomachines, especially when used to

compliment experimental findings. This is the crux of a pair of recent review papers by Adamczyk [1] and Dunn [2] concerning the state of the art in aerodynamic and durability predictions in the gas turbine industry, respectively.

Turbomachinery designers often employ both steady-state and time-resolved predictive tools during the development of new engines. The major difference between the methods is the numerical treatment of the inter-row boundary. For steady-state turbomachinery simulations, common methodologies include the average-passage formulation of Adamczyk [1] and the mixing plane as employed in the Ni code [3-6]. In the latter, the flow from an upstream blade row is circumferentially averaged and then the flow properties are passed into the downstream row as a radial profile. For many situations the difference between the steady-state flowfield and the time-average of an unsteady solution is minor. However, it is the time-resolved information that is often of critical importance to the designer, as in the case of predicting resonant stresses in the machine.

Predicting the time-resolved behavior of the engine requires the transport of discrete flow structures from one airfoil row into an adjacent airfoil row. The steady-state practice of averaging flows between airfoil rows of different rotation speeds acts to smear out the discrete structure, thus eliminating its specific influence on the system. An unsteady CFD simulation passes information between airfoil rows as a complete 2-D profile, thus maintaining any discrete flow structures present in the flowfield and allowing their influence on downstream airfoil rows.

Examples of such discrete flow structures are airfoil wakes, potential fields, and shocks that can travel downstream and/or upstream through the engine [7]. Turbine airfoil surfaces constantly encounter fluctuating flowfields induced by such flow structures. These can manifest as pressure fluctuations that impart time-varying forces which result in the generation of cyclic rotor vibratory stresses that have the potential to reduce the life of the airfoil. Design methodologies are constantly being improved to predict these airfoil vibratory stresses, and such computations are now routinely performed in the design cycle at some companies [8-11]. The time-varying pressure field, as predicted using unsteady simulations, is critical to this effort, and hence a robust technique for ensuring the validity of the computations is a necessity.

In terms of engine performance, a number of studies have involved the intentional shifting of circumferential position between successive blade and/or vane rows [12-15]. Known as airfoil clocking, this relative difference in circumferential position is used to control the location of upstream airfoil wakes as they propagate through downstream airfoil passages in order to achieve a performance benefit in terms of increased efficiency. Such calculations rely on the structure of an airfoil wake to remain intact as it progresses downstream through the engine. Again, the presence of a mixing plane would average-out the wake structure between airfoil rows and hence would eliminate the ability of the simulation to predict clocking effects.

Another phenomenon of concern involves the interaction of a combustor hot-streak with the downstream rows of the turbine [16-19]. Hot-streaks have the potential to impact negatively the life of downstream airfoil rows if not anticipated during the turbine design phase. Unsteady CFD provides a means to track the development of a combustor hot-streak as it persists through the turbine, thereby identifying which airfoils are at risk for a hot-streak encounter and predicting the potential impact on airfoil life.

There are well established means for determining the accuracy of CFD simulations with respect to grid- and time-step convergence [20, 21]. This has led to policy statements from the engineering societies with respect to code verification and validation in general [22] and numerical accuracy in particular [23]. Of interest here is "iterative convergence." The policy statement from the ASME *Journal of Fluids Engineering* [23] states that, "stopping criteria for iterative calculations must be precisely explained, [and] estimates must be given for the corresponding convergence error." Iterative convergence criteria for steady-state simulations are well established: convergence is typically measured by tracking the iteration-to-iteration change of one or more flowfield quantities and looking for this value either to drop below a minimum threshold or to reach a zero slope. In an unsteady CFD simulation, the time-periodic nature of the flowfield precludes such a measure of convergence so some other technique is required.

In the gas-turbine industry designers often make simple qualitative judgments as to periodicity of the flow, and this is seldom based on interrogation of more than a few signals. Further, in most publications, discussion of unsteady convergence is cursory. One exception is due to Laumert et al. [24], who defined convergence of their unsteady simulation as occurring when the maximum deviation in static pressure between two periodic intervals was less than 0.1% over the airfoil surface at midspan. More recently, Ahmed and Barber [25] defined unsteady convergence in terms of time-varying Fast Fourier Transform (FFT) magnitudes calculated as the solution progresses. As time-resolved flowfield predictions become an ever increasing part of physics-based design systems the need for quantitative measures of iterative convergence becomes critical. This is particularly true when time-resolved CFD is used during detailed design where both rapid turn-around time and predictive accuracy are critical.

Design-optimization systems are becoming more and more prevalent within the industry [26], and using time-accurate CFD within such a system necessarily requires quantitative convergence monitoring. During a typical optimization study, the largest bottleneck is the computational time required to obtain a valid solution when considering the currently-perturbed design parameter. Without a converged solution from which to extract one or more parameters used in an objective (or fitness) function, it is not possible to determine a correct relationship between the perturbed design parameters and the design objective. One is left with little choice but to set each optimization perturbation to run a high number of iterations to ensure convergence. Consequently, the potential savings in the wall-clock time required to achieve a given objective is significant if a time-resolved convergence criterion is available.

A robust, quantitative process for assessing the level of convergence of a time-accurate simulation is required. Ideally, the method should consist of calculations that both track the progress of the simulation and allow for the detection of inherent unsteadiness in the flowfield. Here we define a measure of time-periodic convergence and apply the technique

to a number of unsteady simulations relevant to modern gas-turbine design. Again, application of the technique ensures the effective usage of time-accurate analyses during traditional design exercises and enables effective unsteady optimization.

QUALITIES OF AN UNSTEADY CONVERGENCE CRITERION

Often in flowfield predictions in turbomachines, the period of the most significant unsteady fluctuations is expected from the circumferential interval modeled and the known wheel speed. During the execution of the time-accurate simulation, various aspects of the flowfield can be monitored at discrete intervals equal to some multiple of the computational time step. One can then calculate time-mean and time-resolved quantities of interest, and these may include but are not limited to the mass flow rates through domain inlet and exit boundaries, total pressures and temperatures (to obtain aero-performance), and static pressures on airfoil surfaces (to calculate resonant stresses). The collection of these quantities over the iteration history of the solution provides a set of discrete, time-varying signals which can be processed using standard signal processing techniques. Here, a set of signal processing operations, described in more detail by Ifeachor and Jervis [27] and in [28], were selected carefully for their relevance to both the design process in general and the case of periodic unsteadiness in particular.

As mentioned above, designers primarily perform unsteady simulations either to determine the effect of design changes on the time-mean characteristics of the machine (e.g. aero-performance or heat load) or to estimate resonant stresses on the airfoils. So, the development of both time-mean and time-resolved quantities is important for unsteady convergence monitoring. It is straightforward to track the former over periodic intervals, but the latter requires some consideration. Resonant stress analyses are typically performed at discrete engine orders consistent with the Campbell diagram of the airfoil row [9]. Such calculations require accurate information on the unsteady forces on the airfoil row implying both magnitude and phase information at the frequencies of interest. These frequencies are driven by the airfoil counts in the machine where both the fundamental frequencies and a number of harmonics may be important. So, it is necessary at a minimum to track the development of the magnitude and phase of relevant frequencies from periodic interval to periodic interval as well as time-mean quantities.

An effective convergence criterion for unsteady flows also allows for the possibility of inherent unsteadiness existing in a flowfield. This often occurs in turbomachinery as a consequence of vortex shedding at the trailing edge of the airfoil. Such shedding can occur whether or not a significant separation zone exists on the airfoil suction surface, and the frequency is dictated by the relevant Strouhal number of the flow over the airfoil. Fortunately, two other signal analysis measures, cross-correlation and the power spectral density, are useful under such circumstances.

One can cross-correlate a time-varying signal determined over one expected periodic interval with the same signal calculated over the next period. The result is itself a repeating signal that should have the same period as that expected in the simulation. Further, the magnitude of the cross-correlation coefficient at zero lag is a direct measure of how alike the signal is over each of the pair of expected periodic intervals. If significant inherent unsteadiness exists in the flowfield, then the magnitude at zero lag can be significantly less than one, and the period of the cross-correlation coefficient can occur at a number of lags that is inconsistent with that expected in the simulation.

In signal processing Parseval's theorem states that the integral of the power spectral density over a defined range of frequencies is equal to the contribution of fluctuations on that interval to the overall mean square of the signal. Consequently, one can sum the power spectral densities over all significant frequencies expected in the simulation and compare that to the overall mean square. If the summed signal power is not a large fraction of the overall signal variance, then either inherent unsteadiness exists in the flowfield or a higher harmonic of the fundamental passing frequencies is more significant than expected. Of course, it is also possible to use the level of the power spectral density to determine the frequencies associated with the inherent unsteadiness and/or the higher harmonics, and one can then alter the execution of the unsteady simulation (and subsequent post-processing and resonant stress analysis) accordingly.

It is clear that all of the above measures are important for an assessment of unsteady convergence, and a means for combining all the relevant information into a single measure may be obtained from the field of fuzzy logic. Klir et al. [29] describe the process of "fuzzy decision making" that applies in situations such as these, and Clark and Yuan [30] have previously used the method to detect the edges of turbulent spots in a transitional flowfield consistent with a turbine blade. Further details regarding decision making with fuzzy sets can be found in Zimmermann [31] and Klir and Yuan [32]. The process employed here is described below along with complete details of the convergence assessment method.

A METHOD FOR UNSTEADY CONVERGENCE ASSESSMENT

It is useful to describe the details of the current method with respect to an example periodic-unsteady simulation. A machine that is convenient for this purpose is the AFRL High Impact Technologies Turbine Rig (HITTR). An early design iteration of the turbine, denoted here as HPT1, is described in detail by Johnson [33]. The geometry is a single-stage high-pressure turbine consistent with an engine cycle envisaged for 2017 and beyond. The vane and blade airfoil counts of HPT1 are 22 and 44, respectively. The turbine was analyzed via the 3D time-accurate Reynolds-Averaged Navier Stokes (RANS) solver of Dorney and Davis [34], which is itself a further development of the Rai code [35, 36].

The turbine geometry is shown in Fig. 1 as the portion of the wheel ($1/22^{nd}$) modeled in the simulation. Colorization of the non-slip surfaces in the figure is based on instantaneous static pressure. The wheel speed at conditions consistent with a short-duration rig experiment for design-system code validation in the AFRL Turbine Research Facility [37, 38] is 7050 rpm, and with $1/22^{nd}$ of the annulus modeled the expected periodicity occurs on an interval equal to approximately 0.387 ms. This interval corresponds to one vane-passing per blade or the passage of two blades per vane. At the time-step depicted in Fig. 2, the simulation had completed approximately 19 periodic cycles (vane passings), and the time-varying pressure at the

location indicated on the blade pressure side for the 2 subsequent cycles is plotted in Fig. 2a. While a surface static pressure on the blade pressure side is used in the present example, it is possible to use the method with any flow variable at any location of interest in the domain that is relevant to the design issue at hand.

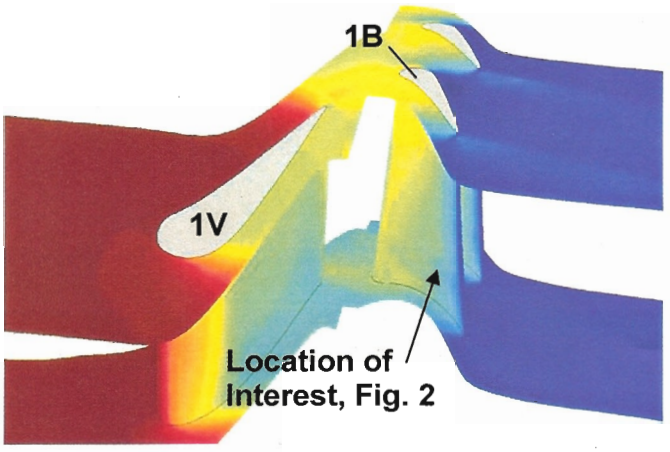

Figure 1. Instantaneous static pressure on the no-slip surfaces of the HIT Turbine Rig simulation (HPT1).

All signal-analysis operations required to apply the convergence-assessment method are illustrated in Fig. 2a-2e. Again, these are the calculation of the time-mean of the flow quantity over each periodic cycle, the Discrete Fourier Transform (DFT), the cross-correlation coefficient (CCF), and the power spectral density (PSD). The time-mean of the static pressure over a single periodic cycle is

$$\overline{p} = \frac{1}{N}\sum_{n=0}^{N-1} p(n+1) \tag{1}$$

where N is the number of times steps per period and $p(n+1)$ is the static pressure calculated at an integer multiple, $n+1$, of the time step, Δt. In Fig. 2(a) the time-mean levels calculated over each of the two periodic cycles are plotted as well as the raw pressure trace. Complete convergence of the time-averaged signal is achieved when there is no difference in signal mean from one periodic interval to the next.

The Discrete Fourier Transform of the fluctuating pressure, p', evaluated at an integer multiple, $k+1$, of the signal sampling frequency, $\Delta f = (N \Delta t)^{-1}$ is given by

$$P(k+1) = \sum_{n=0}^{N-1} p'(n+1)\, e^{-i\frac{2\pi k n}{N}} \tag{2}$$

where Fourier components are defined for values of k between 0 and N-1. Each Fourier component is a phasor,

$$P(k+1) = \mathrm{Re} + \mathrm{Im}\, i \tag{3}$$

and the time-periodic fluctuation at a given multiple of the sampling frequency can be reconstructed by

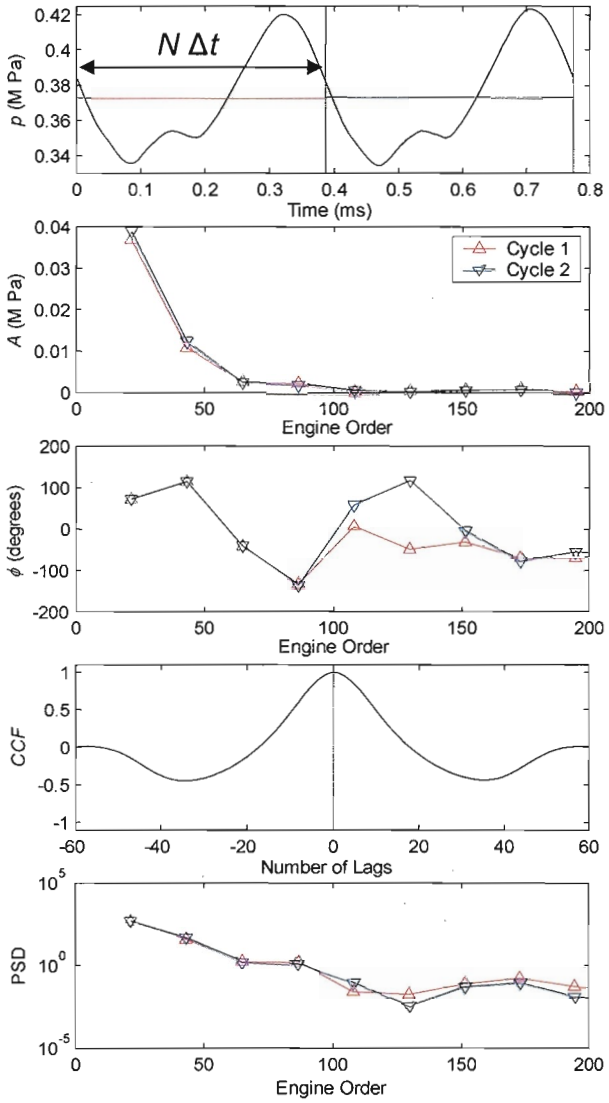

Figure 2. An example of signal-analysis techniques used in the current method for HPT1: (a) time mean, (b) DFT magnitudes and (c) phase angles, (d) cross-correlation coefficients, and (e) power-spectral densities.

$$p(t) = \mathrm{Re}\left\{ A e^{i(\omega t + \phi)} \right\} = A\cos(\omega t + \phi). \tag{4}$$

In Equation 4, A is the normalized DFT magnitude, given by

$$A = 2\left(\mathrm{Re}^2 + \mathrm{Im}^2\right)^{\frac{1}{2}} / N \quad , \tag{5}$$

Φ is the phase angle defined as $\tan^{-1}$ (Im / Re), and ω is the circular frequency corresponding to the integer multiple of the sampling frequency, $2\,\pi\,\Delta f\,(k+1)$. DFT magnitudes and phase angles are plotted in Figs. 2(b) and 2(c), respectively for each of the periodic intervals plotted in Fig. 2(a). Convergence of the simulation at a given frequency is complete when there is neither a change in magnitude nor a difference in phase between the DFT results for two consecutive periodic intervals at frequencies of interest to the designer.

The results of a cross-correlation of the signals from the two periodic cycles of Fig. 2(a) are plotted in Fig. 2(d). In the time domain the cross-correlation coefficient (CCF) is given by

$$CCF(L) = \frac{\frac{1}{N}\sum_{n=0}^{N-1} p'((n+1)+L)\, p'((n+1)+N)}{\frac{1}{N}\left[\sum_{n=0}^{N-1} p'^2(n+1) \quad \sum_{n=0}^{N-1} p'^2((n+1)+N)\right]^{\frac{1}{2}}} \quad . \qquad (6)$$

The calculation at a given time lag, L, is accomplished first by multiplying the time-lag-shifted fluctuating pressure over the first interval by the fluctuating pressure signal for the second periodic interval, summing products, and then dividing by the number of samples per period. The result is then normalized by the product of the root-mean-square levels for the two signals. Complete convergence of the unsteady simulation yields a cross-correlation coefficient equal to 1 at zero lag. This implies that the signals from the first and second periodic intervals are exactly alike and that N is the true period of the signals.

The power spectral densities (PSD) of the signals from the two periodic intervals plotted in Fig. 2(a) are shown in Fig. 2(e). The PSD at a given multiple of the sampling frequency is defined as the product of the Fourier component at that frequency and its complex conjugate divided by the number of samples, N. Convergence of a time-resolved turbomachinery simulation occurs when a large fraction of the overall signal power occurs at frequencies of interest and when that portion of the mean square does not change from one periodic interval to the next.

It is useful to calculate a single parameter that can be used to gauge the level of convergence of the simulation, and multi-valued logic provides a convenient means of accomplishing this objective [29]. One can use the calculated time-mean levels, DFT magnitudes and phase angles, cross-correlation coefficients at zero lag, and fraction of overall signal power at frequencies of interest to define a series of fuzzy sets that express various aspects of the degree of convergence. These fuzzy sets are as follows

$$f_M = 1 - \left| 1 - \frac{\bar{p}_2}{\bar{p}_1} \right| \qquad (7)$$

$$f_A = 1 - \left| 1 - \frac{A_2}{A_1} \right| \qquad (8)$$

$$f_\phi = 1 - \left| \frac{\phi_2 - \phi_1}{\pi} \right| \qquad (9)$$

$$f_S = \left| CCF(0) \right| \qquad (10)$$

$$f_P = \frac{\sum_{k=k_{expected}}^{N-1} PSD(k+1)}{\sum_{k=0}^{N-1} PSD(k+1)} \qquad (11)$$

where the subscripts 1 and 2 refer to the first and second cycles, respectively. Evaluation of Equations 7-11 gives membership grades in fuzzy sets that describe consistent mean level, amplitude, phase angle, overall signal shape, and fractional signal power, respectively. The amplitude and phase membership grades of Equations 8 and 9 are calculated for each frequency of interest as defined, for example, by an airfoil Campbell diagram. The numerator in Equation 11 is a summation over all frequencies expected to produce significant signal power in the simulation. A level substantially less than 1 implies the presence of either inherent unsteadiness in the simulation or a significant signal level due to some higher harmonic of the expected fundamental frequencies.

The overall convergence level is then itself a fuzzy set defined as the intersection of the others

$$f_C = f_M \cap f_A \cap f_\phi \cap f_S \cap f_P \quad , \qquad (12)$$

and this is in turn given by the standard fuzzy intersection [29]

$$f_C = \min(f_M, f_A, f_\phi, f_S, f_P) \quad . \qquad (13)$$

Here we define $f_C \geq 0.95$ for two consecutive cycles to be consistent with convergence of the periodic-unsteady flowfield. To continue this example, Equations 7-13 were evaluated for the signals plotted in Fig. 2, and the results are shown in Table 1. For this simulation, significant unsteadiness was expected to occur due to the fundamental vane-passing frequency (22E) as well as two harmonics of that frequency (44E and 66E). Note that more than 99% of the overall signal power is contained in the expected frequencies, so there is not any significant inherent unsteadiness evidenced in the signal. Also note that the signals are 99.9% correlated between the two periodic intervals, so the overall signal shape is very well converged. There is very little phase difference between cycles at the frequencies of interest, and the variation of amplitudes between cycles is greatest for the first harmonic of the fundamental. As a consequence, the overall convergence level of the simulation is 0.886, and this is dictated by the change in amplitude of that engine order (44E) from cycle to cycle.

Table 1. Results of the fuzzy-set convergence analysis as applied to the signals in Fig. 2.

Fuzzy Set	Membership Grade
f_M	0.999
f_A (22E)	0.947
f_Φ (22E)	0.991
f_A (44E)	0.886
f_Φ (44E)	0.990
f_A (66E)	0.933
f_Φ (66E)	0.988
f_S	0.999
f_P	0.997
f_C	0.886

At this point, it is worth noting that the fuzzy sets f_M and f_S taken together are akin to the sort of information that an "expert user" of unsteady CFD employs to judge the convergence of a simulation. Such an expert would typically plot the time-variation of flowfield quantities for two of more periodic cycles and make a judgment as to how alike the DC and AC

components of the signal are from one cycle to the next. In this example, there is very little change in both the time-mean level and the overall signal shape between the cycles plotted in Figure 2. An expert user would undoubtedly come to the same conclusion from a visual inspection of the pressure trace plotted in Figure 2(a). However, one can see in Table 1 that the amplitude of the first harmonic of vane passing is still changing significantly over the two periods plotted in Figure 2(a). Since simulations of this type are often performed to assess vibratory stresses during the design cycle of an engine, there is a clear advantage to the application of a more robust method of convergence assessment like that described here. For example, an 11% variation in the amplitude of unsteady forcing could well mean the difference between passing and failing an FAA certification test for resonant stresses.

To complete this example, Figure 3 is a plot of the fuzzy convergence level versus the periodic cycle number for 34 periodic intervals (i.e. 34 vane-passing events). The fuzzy sets that dictate the outcome of the overall level are also indicated on the figure. One can see that the convergence behavior of the simulation is in this case controlled by the variations of the magnitude and phase of harmonics of the fundamental from cycle-to-cycle. While this convergence behavior is typical of simulations where simple vane-blade interaction effects dominate the flowfield, the importance of tracking more than the Fourier components as the solution progresses is illustrated below with reference to other turbine geometries.

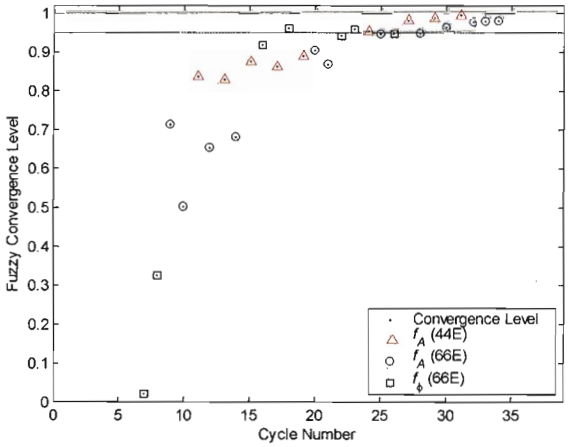

Figure 3. Convergence behavior of the flowfield at the location of interest given in Figure 1 for HPT1.

Again, it is important to recognize that the flowfield parameter selected for convergence monitoring is case dependent: the most important quantities are dictated by the reasons for performing the simulation. If the designer is assessing the expected level of resonant stress due to a specific forcing function on the airfoil surface, then the amplitude and phase angle at that frequency must be monitored at a number of locations on the airfoil surface. Alternatively, the amplitude and phase angle of the integrated aerodynamic load on the surface can be monitored. In addition, if the purpose of the analysis is to quantify a change in the time-mean performance resulting from the latest design iteration, then the mass- or mixed-out-averaged efficiency of the stage is the quantity to monitor.

One must also keep in mind that some quantities within the simulation converge well before others: for example, the pressure field typically becomes truly periodic well in advance of the entropy field due to the disparate propagation rates of finite pressure waves and viscous disturbances. So, great flexibility was built into the implementation of the convergence-assessment algorithm described above. The user can monitor a large number of flow quantities at any point in the flowfield. This is very useful when determining overall simulation convergence in post-processing mode. Also, one can estimate the convergence of arbitrary signals generated as the solution progresses (e.g. mass-flow rates, efficiencies, integrated airfoil loadings, etc.), and that can be used to control an unsteady optimization routine. Further examples of the application of this algorithm to a number of periodic-unsteady flowfields predicted in turbines during the design cycle are described below.

CONVERGENCE BEHAVIOR OF SIMULATIONS OF VANE-BLADE INTERACTION

A primary reason for executing an unsteady CFD simulation during the turbomachinery design cycle is to predict airfoil resonant stresses. If vibratory stress problems are detected early enough during detailed design, then they can be mitigated [9]. However, if unacceptable vibratory stresses are discovered after the engine has been put into service, significant warranty costs could be involved if changes to the geometry are required. Avoidance of design escapes is thus critically dependent upon accurate predictions of unsteady loads on airfoil surfaces.

Predictive tools for vibratory stresses rely on accurate Fourier analysis of time-resolved pressure fields [8, 10], and true periodicity is required to avoid errors resulting from spectral leakage [27]. Thus it is necessary for designers to quantify convergence levels prior to determining vibratory stresses. When predicting a flowfield to assess vibratory stresses, time-resolved traces of the integrated airfoil loading provide a suitable means to monitor convergence. Airfoil surface static pressure fluctuations are the root cause of vibratory stresses, and when integrated over the airfoil surface, these static pressures provide the airfoil loading.

As an example, a stage-and-one-half calculation was performed for a high-pressure turbine (HPT2) with 48 1st vanes, 72 1st blades, and 84 2nd vanes, modeled as 1/12th of the full-wheel geometry. Based on these airfoil counts, one would expect blade vibratory stresses to arise due to the 48E and 84E vane-passing frequencies as well as their harmonics. However, it is unlikely that resonant crossings due to frequencies larger than 168E would occur in the operating range of the turbine. So, the fundamental and first harmonic of each vane-passing frequency is considered in the analysis.

Figure 4 is a plot of the convergence level, f_C, calculated using integrated blade loadings on a cycle-by-cycle basis for the high-pressure turbine blade. Separate values of f_C were calculated for each of the time-trace signals representing the axial, tangential, and radial forces on the blade as well as the bending moment. One can see that the integrated blade loadings are very well converged after 5 periodic cycles with

values of f_C greater than 0.95 for all force components as well as the moment.

Convergence of the blade integrated loading occurs rapidly in this example, and that is an indication that the unsteadiness in static pressure is primarily driven by potential field and/or shock interaction effects. The propagation rate of viscous disturbances in a turbine flowfield is much smaller than that of finite pressure waves, so one would expect that the level of convergence of total quantities entering and exiting the blade row is correspondingly lower at a given periodic cycle. Inspection of Figure 5 confirms this supposition. The figure is a plot of convergence levels for inlet and exit mass-flow rates as well as total pressures and temperatures. For all periodic cycles a comparison of f_C levels between Figures 4 and 5 indicates that the static pressure field of the turbine converges faster than the viscous flowfield. Therefore, if the current example were used to determine the effect of a design change (e.g. vane clocking) on unsteady loss levels as well as to predict resonant stresses, then the simulation requires a longer run time prior to post-processing.

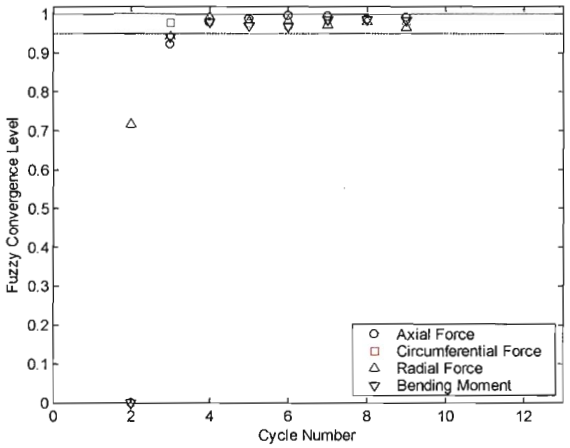

Figure 4. Convergence levels for blade force components as a function of periodic cycle for HPT2.

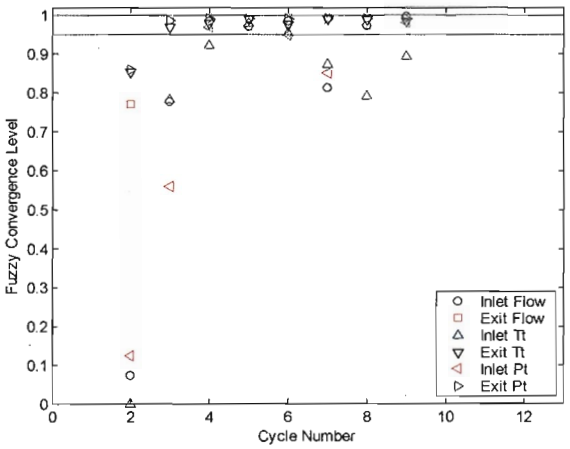

Figure 5. Convergence of flow rates, total pressures, and total temperatures at the blade inter-row boundaries for HPT2.

For another example of the performance of the present method, consider a stage-and-one-half calculation for a high-pressure turbine (HPT3) having airfoil counts equal to 36, 72, and 48 in the first vane, first blade, and second vane row, respectively. Again, $1/12^{th}$ of the wheel was modeled in the simulation with the purpose of the analysis to assess drivers due to the fundamental vane-passing frequencies only. The solution was run for 6 complete cycles, and that was enough to yield convergence of the unsteady loadings in the previous example. However, inspection of Figure 6 reveals that convergence was not achieved on that interval in the current example. In fact, a convergence level of less than 0.7 was achieved for the axial force component.

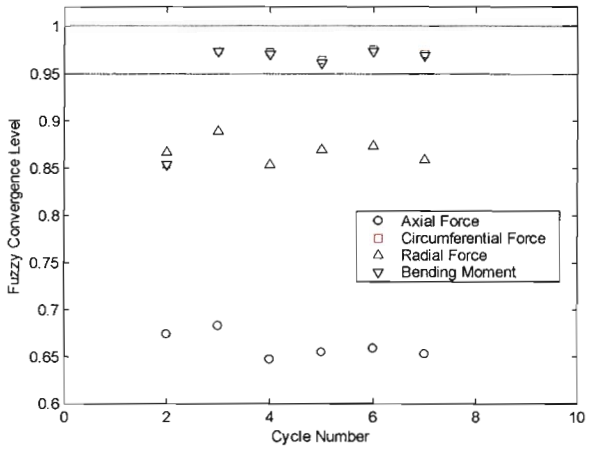

Figure 6. Convergence levels for blade force components as a function of periodic cycle for HPT3.

Since the level of convergence achieved by the axial component was lower than that of all the others, it was selected for further investigation. Figure 7 is a plot of the normalized axial force signal as well as the membership grades in the fuzzy sets defined in Equations 7-11 as a function of periodic cycle number. The convergence level is dictated by the lowest membership grade over all the membership functions, namely, the fractional signal power, f_P. A low level of f_P implies that there is significant unsteadiness due to an unexpected frequency. Also note that low levels of the cross-correlation at zero lag, f_S were obtained. This implies a significant change in signal shape from cycle-to-cycle, and this can mean that the primary periodicity occurs in the simulation over some unanticipated time-scale, calling into question the validity of the DFT results used throughout the method. In any case, the results suggest that rigorous interrogation of the unsteady flowfield predicted in the turbine is warranted.

Figure 8 is a plot of fractional signal power due to engine orders of excitation up to 300. There is significant unsteadiness in the axial force exerted on the blade due to the first harmonic of the second-vane passing frequency, and this contributes to the low level of f_P. Consideration of the blade Campbell diagram might lead one to conclude that no resonance is to be expected due to that forcing function. However, more problematic is the signal power detected at the engine orders above 150. While 180E is the fourth harmonic of the first-vane passing frequency, the significant peak that occurs at 168E is spurious, and it warrants further investigation.

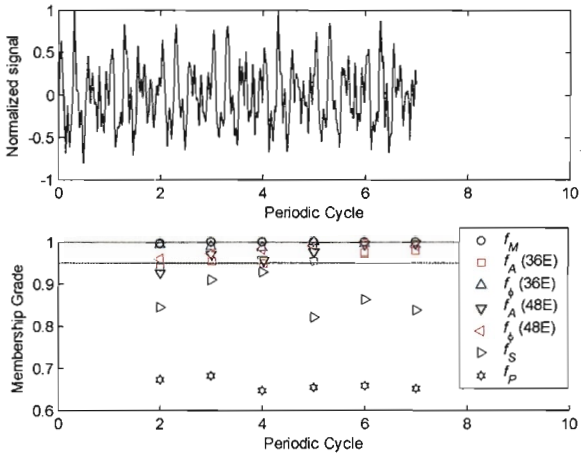

Figure 7. Plots of time-resolved blade axial force and fuzzy-set membership grades as functions of the periodic cycle (HPT3).

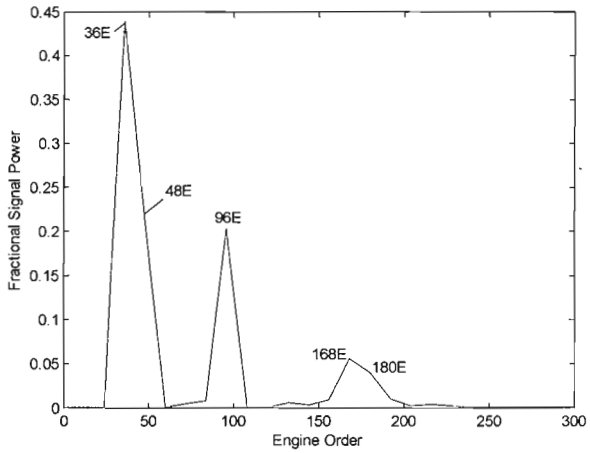

Figure 8. The results of a PSD analysis performed on cycle seven of the axial force signal for the blade of HPT3. Power contributions from unexpected frequenceies are apparent.

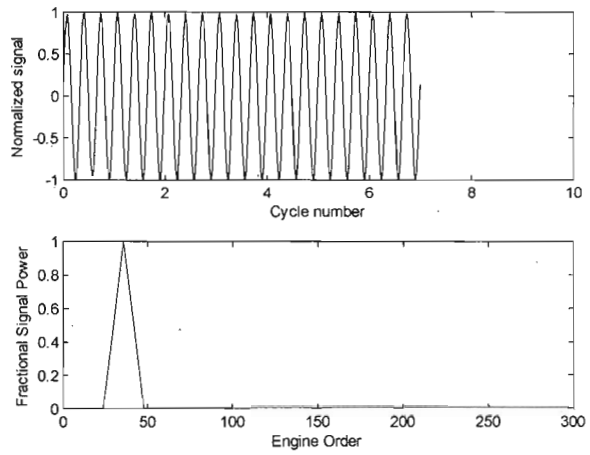

Figure 9. Normalized flow-rate into the blade row versus periodic cycle number and the results of a PSD analysis of the signal (HPT3).

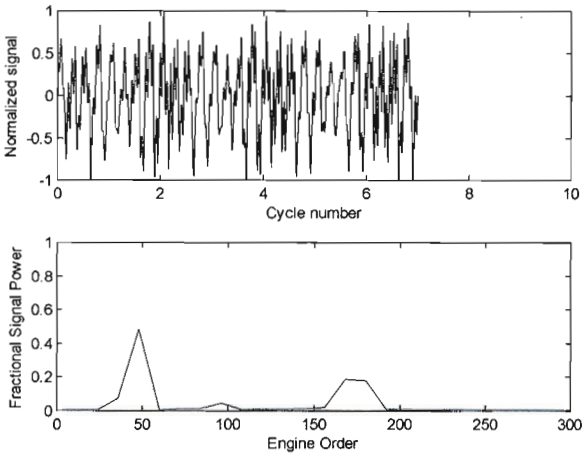

Figure 10. Normalized flow-rate out of the blade row versus periodic cycle number and the results of a PSD analysis of the signal (HPT3).

Plots of normalized, time-resolved flow rates entering and exiting the blade row are plotted in Figures 9 and 10, respectively, along with fractional signal power as functions of frequency resulting from PSD analysis. One can see the unsteady blockage effect of the upstream vanes very clearly in the inlet flow plots of Figure 9. In Figure 10, however, there is significant unsteadiness associated with the blockage of the downstream airfoils as well as high-frequency unsteadiness at 168E and 180E. A high-frequency blockage effect is suggestive of inherent unsteadiness (i.e. vortex shedding). Further, the unsteadiness is broad-banded and suggests that the shedding is actually occurring at a frequency between 168E and 180E with an attendant picket-fencing effect on the spectral analysis.

One can see additional evidence of vortex shedding in Figures 11 and 12. Figure 11 is a plot of the DFT magnitude calculated from the time-resolved entropy rise through the blade row at 168E ($\approx$ 31 kHz). A midspan plane is shown for a single blade passage, and the highest magnitude of the unsteady entropy rise is found in the vicinity of the blade trailing edge. Again, this is characteristic of vortex shedding. A calculation of the Strouhal number of the oscillations based on trailing-edge diameter and the local velocity in the vicinity of the trailing edge gives a value of ≈ 0.16. Figure 12 is a plot of the local DFT magnitude of unsteady static pressure at the same midspan plane for the 168E frequency. High levels of unsteady static pressure occur near the blade throat and downstream of the trailing edge at a location consistent with a reflected cross-passage shock. It is concluded that the unsteady blockage caused by the vortex shedding produces enough of an instantaneous variation in the throat area to cause a shock to form. Consequently exceptionally high levels of unsteady pressure occur on the blade suction side at the vortex-shedding frequency.

Note that the simulation described above represents an early iteration in the design cycle for a turbine. In part as a consequence of these results, the design parameters of the turbine changed markedly before the final geometry was obtained. Consequently, no significant high-frequency unsteadiness occurred in the product. So, it is unclear whether

or not the phenomenon described here could in fact lead to an airfoil failure. However, Doorly and Oldfield [39] have noted the presence of instantaneous local separation on a turbine blade in conjunction with shock passing, and their Schlieren images were suggestive of the occurrence of the phenomenon described here in the vicinity of the blade trailing edge. In any case, it is clear from this example that application of the present method to assess convergence in predictions of vane-blade interaction provides designers and analysts with significant direction as to the interrogation of the flowfield and the health of the design.

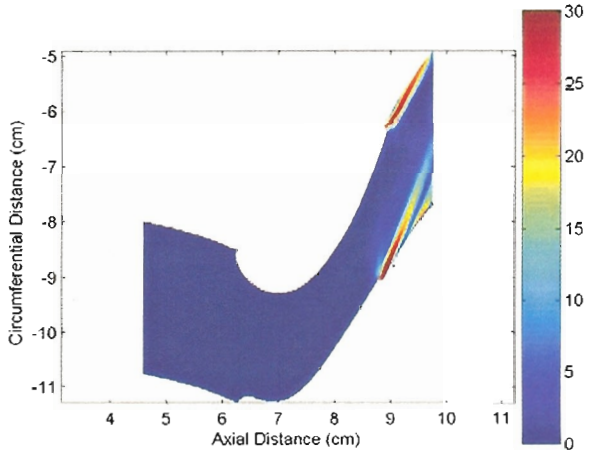

Figure 11. Contours of DFT magnitude at 168E calculated from time-resolved entropy rise (J / kg / K) at midspan through the blade passage (HPT3).

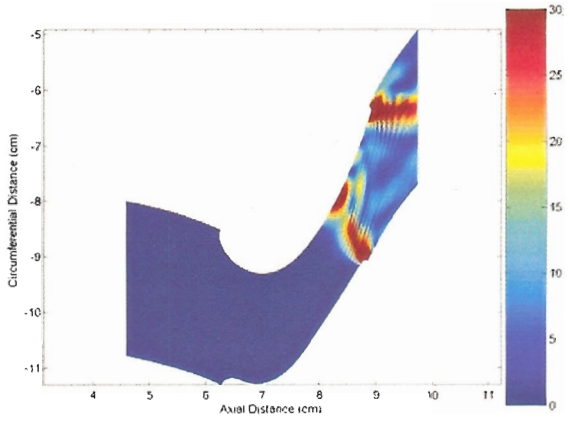

Figure 12. Contours of DFT magnitude at 168E calculated from time-resolved static pressure (k Pa) at midspan through the blade passage (HPT3).

CONVERGENCE BEHAVIOR OF SIMULATIONS OF HOT-STREAK MIGRATION

During the design cycle, unsteady analysis is used to assess the effect of hot streaks on the aero-performance and durability of downstream rows, and one can employ the present method to judge convergence in such flowfields. As an example, consider a simulation of hot-streak migration through the first stage of another high pressure turbine (HPT4). The geometry consists of a vane/blade configuration with a combustor thermal exit-profile mapped onto the vane inlet boundary. The CFD model contains 48 stator airfoils and 72 rotor airfoils as well as 24 regions of distinctly higher-enthalpy fluid corresponding to the location of the combustor nozzles. The hot-streaks are aligned with the leading edges of alternating vanes, and one third of the hot-streaks are at an elevated temperature with respect to the other two thirds. The remainder of the inlet profile is adjusted to maintain a given area averaged inlet total temperature. Contours of local total temperature are shown in Figure 13.

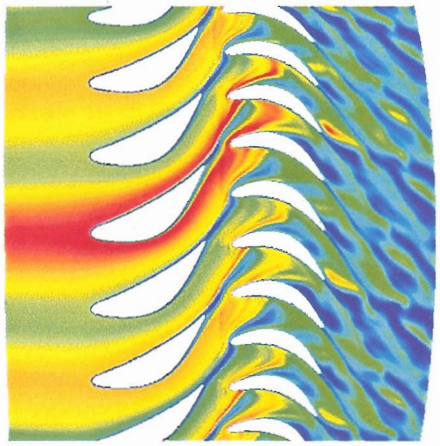

Figure 13. Instantaneous total temperatures through HPT4 for the hot-streak simulation.

For such a configuration, the convergence of the system should be calculated using rotor-based quantities. As the blades traverse behind the circumference of the vane ring, they pass through a number of regions of alternating enthalpy as well as the vane wakes, and the blade flowfield responds accordingly. Further, one might hypothesize that for a well designed vane row at subsonic vane exit Mach number, the hot streaks comprise the major sources of unsteadiness for the blade airfoils. So, Figure 14 is a plot of convergence levels versus periodic cycle number for the inlet- and exit mass-flow, total temperature, and total pressure obtained by considering the 8E, 24E, and 48E drivers as dominant. In Figure 14 good levels of convergence are seen for all quantities except the upstream total pressure.

A power-spectral analysis of the upstream total pressure signal is plotted in Figure 15 along with the time-variation of that quantity, normalized by the peak value. One can see that all signal power in the upstream total pressure trace comes not from the hot-streaks (8E and 24E) but from the vane wakes (48E and 96E), and this is consistent with the Munk and Prim [40] substitution principle. Accordingly, the effect of the hot streaks is not seen in the comparatively steady aerodynamics of the vane: instead, it is manifested in the unsteady flow through the blade row [16, 17]. A final check of the convergence behavior of the case with respect to the tangential component of the force on the blade is presented in Figure 16. The membership grades of all the fuzzy sets are greater than 0.95 by the fifth cycle, and this confirms that the case is approaching true periodicity with respect to the blade loading.

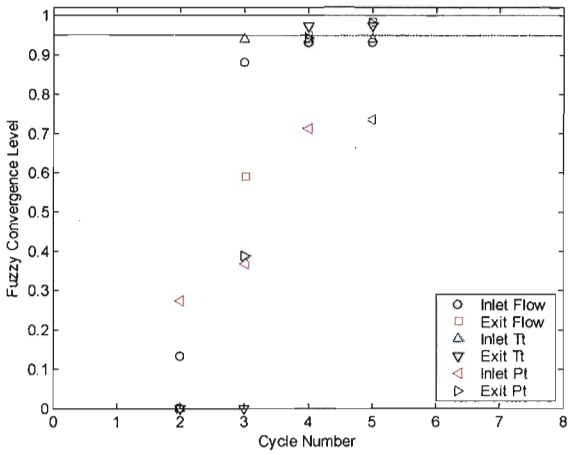

Figure 14. Convergence levels for the blade flowfield variables considering the 8E and 24E frequencies associated with the hot-streak inlet profile (HPT4).

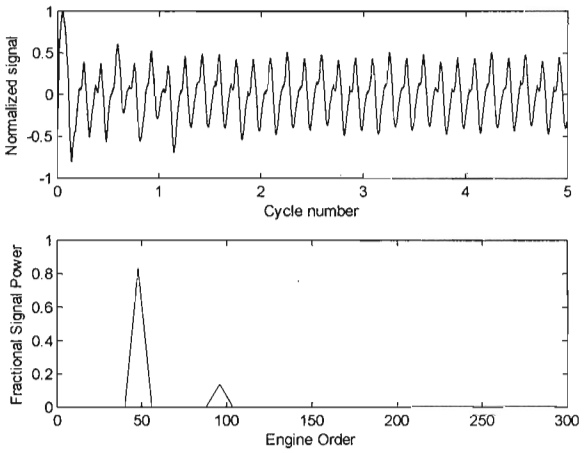

Figure 15. Normalized total pressure upstream of the blade row versus cycle number and a PSD analysis of the signal (HPT4).

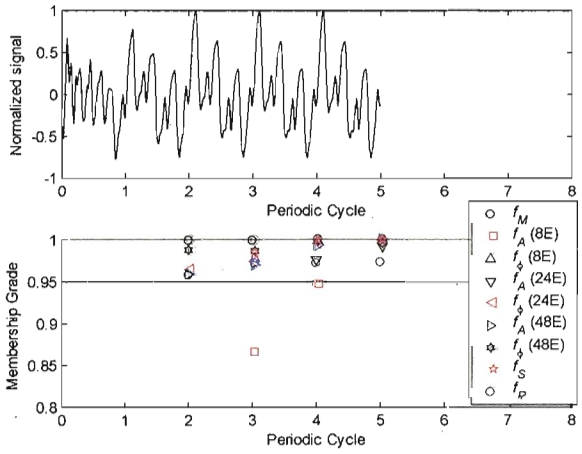

Figure 16. Plots of time-resolved blade tangential force and fuzzy-set membership grades as functions of the periodic cycle (HPT4).

CONCLUSIONS

A quantitative method to assess the level of convergence of a periodic-unsteady simulation was described. The method was based on well known signal-processing techniques, and these were used in conjunction with fuzzy set theory to define a single overall convergence level of the simulation. The development of the method was illustrated with reference to a prediction of vane-blade interaction in a transonic high pressure turbine. The robustness of the technique was then demonstrated by application to a number of simulations consistent with turbine aero-thermodynamic design in industry. It was shown that the technique is very useful as an indicator of the overall quality of the simulations as well as guide to further investigations of the flowfield and characterization of the design. For example, the method was shown to be useful in detecting inherent unsteadiness in the prediction of the flow through a high-pressure turbine, and therefore judicious application of the technique can be a significant factor in preventing design escapes.

ACKNOWLEDGMENTS

The impetus for this work came from discussions that the authors had with Mr. R. K. Takahashi of Mitsubishi Heavy Industries. The authors would also like to thank Mr. Joel Wagner of Pratt & Whitney as well as the three anonymous reviewers for their helpful suggestions to improve the manuscript. Those interested in applying this method to specific problems may contact john.clark3@wpafb.af.mil.

REFERENCES

[1] Adamczyk, J. J., 2000, "Aerodynamic Analysis of Multi-Stage Turbomachinery Flows in Support of Aerodynamic Design," ASME Journal of Turbomachinery, Vol. 122, pp. 189-217.

[2] Dunn, M. G., 2001, "Convective Heat Transfer and Aerodynamics in Axial Flow Turbines," ASME Journal of Turbomachinery, Vol. 123, pp. 637-686.

[3] Ni, R. H., 1982, "A Multiple-Grid Scheme for Solving the Euler Equations," AIAA Journal, Vol. 20, No. 11, pp. 1565-1571.

[4] Ni, R. H. and Bogoian, J. C., 1989, "Prediction of 3-D Multistage Turbine Flow Field Using a Multiple-Grid Euler Solver," AIAA Paper No. 89-0203.

[5] Ni, R.H., "Advanced Modeling Techniques for New Commercial Engines," 1999, XIV ISOABE Conference, Florence, Italy, 5-10 September.

[6] Davis, R. L., Shang, T., Buteau, J., and Ni, R. H., 1996, "Prediction of 3-D Unsteady Flow in Multi-Stage Turbomachinery Using an Implicit Dual Time-Step Approach," AIAA Paper No. 96-2565.

[7] Tyler, J. M. and Sofrin, T. G., 1970, "Axial Flow Compressor Noise Studies," SAE Transactions, Vol. 70, pp. 309-332.

[8] Hilbert, G. R., Ni, R. H., and Takahashi, R. K., 1997, "Forced-Response Prediction of Gas Turbine Rotor Blades," ASME Winter Annual Meeting.

[9] Clark, J. P., Aggarwala, A. S., Velonis, M. A., Magge, S. S., and Price, F. R., 2002, "Using CFD to Reduce Resonant Stresses on a Single-Stage, High-Pressure Turbine Blade," ASME GT2002-30320.

[10] Green, J. S. and Marshall, J. G., 1999, "Forced Response Prediction Within the Design Cycle," IMechE Conference Transactions 1999-1A, pp. 377-391.
[11] Weaver, M. M., Manwaring, S. R., Abhari, R. S., Dunn, M. G., Salay, M. J., Frey, K. K., and Heidegger, N., 2000, "Forcing Function Measurements and Predictions of a Transonic Vaneless Counter-Rotating Turbine," ASME Paper No. 2000-GT-375.
[12] Huber, F., Johnson, P. D., Sharma, O. P., Staubach, J. B., and Gaddis, S. W., 1996, "Performance Improvement Through Indexing of Turbine Airfoils: Part 1- Experimental Investigation," ASME Journal of Turbomachinery, Vol. 118, pp. 630-635.
[13] Griffin, L. M., Huber, F. W., and Sharma, O. P., "Performance Improvement Through Indexing of Turbine Airfoils: Part 2- Numerical Simulation," ASME Journal of Turbomachinery, Vol. 118, pp. 636-642.
[14] Dorney, D. J., and Sharma, O. P., 1996, "A Study of Turbine Performance Increases Through Clocking," AIAA Paper No. 96-2816.
[15] Haldeman, C. W., Dunn, M. G., Barter, J. W., Green, B. R., and Bergholz, R. F., 2004, "Experimental Investigation of Vane Clocking in a One and ½ Stage High Pressure Turbine, ASME Paper No. GT2004-5347.
[16] Shang, T. and Epstein, A. H., 1997, "Analysis of Hot Streak Effects on Turbine Rotor Heat Load," ASME Journal of Turbomachinery, Vol. 119, No. 3, pp. 544-553..
[17] Takahashi, R. K., Ni, R. H., Sharma, O. P., and Staubach, J. B., 1996, "Effects of Hot Streak Indexing in a 1-1/2 Stage Turbine," AIAA Paper No. 96-2796.
[18] Dorney, D. J., and Gundy-Burlet, K., 2000, "Hot-Streak Clocking Effects in a 1-1/2 Stage Turbine," AIAA Journal of Propulsion and Power, Vol. 12, No. 3, pp. 619-620.
[19] He, L., Menshikova, V., and Haller, B. R., "Influence of Hot Streak Circumferential Length-Scale in a Transonic Turbine Stage," ASME Paper No. GT2004-53370.
[20] Roache, P. J., 1998, Verification and Validation in Computational Science and Engineering, Hermosa Publishers, Albuquerque, NM, USA.
[21] Gokaltun, S., Skudarnov, P. V., and Lin, C-X., 2005, "Verification and Validation of CFD Simulation of Pulsating Laminar Flow in a Straight Pipe," AIAA Paper No. 2005-4863.
[22] Guide for the Verification and Validation of Computational Fluid Dynamics Simulations, AIAA Policy Paper G-077-1998, AIAA, Reston, VA, USA.
[23] Freitas, C. J., 1993, "Editorial Policy Statement on the Control of Numerical Accuracy," ASME *Journal of Fluids Engineering*, Vol. 115, No. 2, pp. 339.
[24] Laumert, B., Martensson, H, and Fransson, T. H., 2001, "Investigation of Unsteady Aerodynamic Blade Excitation Mechanisms in a Transonic Turbine Stage, Part I: Phenomenological Identification and Classification," ASME Paper No. 2001-GT-0258.
[25] Ahmed, M. H. and Barber, T. J., 2005, "Fast Fourier Transform Convergence Criterion for Numerical Simulations of Periodic Fluid Flows," AIAA Journal, Vol. 43, No. 5, pp. 1042-1052.
[26] Staubach, J. B., 2003, "Multidisciplinary Design Optimization, MDO, the Next Frontier of CAD/CAE in the Design of Aircraft Propulsion Systems," AIAA Paper No. 2003-2803.
[27] Ifeachor, E. C. and Jervis, B. W., 1996, Digital Signal Processing, Addison-Wesley, New York.
[28] Signal Processing Toolbox User's Guide, Version 5, 2000, The Mathworks, Natick, MA.
[29] Klir, G.J., St. Clair, U.H., and Yuan, B., 1997, Fuzzy Set Theory: Foundations and Applications, Prentice Hall PTR, Upper Saddle River, NJ.
[30] Clark, J.P. and Yuan, B., 1998, "Using Fuzzy Logic to Detect Turbulent/Non-Turbulent Interfaces in an Intermittent Flow," Intelligent Automation and Control, Vol. 6, pp. 113-118, TSI Press, Albuquerque, NM
[31] Zimmermann, H. J. 1990, Fuzzy Set Theory and Its Applications, Second Edition, Kluwer, Boston, MA.
[32] Klir, G. J. and Yuan, B., 1995, Fuzzy Sets and Fuzzy Logic: Theory and Applications, Prentice Hall PTR, Upper Saddle River, NJ.
[33] Johnson, P. D., 2005, "Consortium Turbine Research Rig, Aerothermal and Mechanical Design," AFRL Technical Report AFRL-PR-WP-TR-2005-2157.
[34] Dorney, D. J. and Davis, R. L., 1992, "Navier-Stokes Analysis of Turbine Blade Heat Transfer and Performance," ASME Journal of Turbomachinery, Vol. 114, pp. 795-806.
[35] Rai, M. M., 1987, "Navier-Stokes Simulations of Rotor-Stator Interaction Using Patched and Overlaid Grids," AIAA Journal of Propulsion and Power, Vol. 3, pp. 387-396.
[36] Rai, M. M. and Madavan, N. K., 1990, "Multi-Airfoil Navier-Stokes Simulations of Turbine Rotor-Stator Interaction," ASME Journal of Turbomachinery, Vol. 112, pp. 377-384.
[37] Polanka, M.D., Hoying, D.A., Meininger, M., and MacArthur, C.D., 2003, "Turbine Tip and BOAS Heat Transfer and Loading, Part A: Parameter Effects Including Reynolds Number, Pressure Ratio and Gas to Metal Temperature Ratio", ASME Journal of Turbomachinery, Vol. 125, pp. 97-106.
[38] Clark, J. P., Polanka, M. D., Meininger, M., and Praisner, T. J., 2006, "Validation of Heat-Flux Predictions on the Outer Air Seal of a Transonic Turbine Blade," accepted for publication in the ASME Journal of Turbomachinery.
[39] Doorly, D. J. and Oldfield, M. L. G., 1985, "Simulation of the Effects of Shock Wave Passing on a Turbine Rotor Blade," ASME Journal of Engineering for Gas Turbines and Power, Vol. 107, pp. 998-1006.
[40] Munk, M. and Prim, R., 1947, "On the Multiplicity of Steady Gas Flows Having the Same Streamline Pattern," Proceedings of the National Academy of Sciences, Vol. 33, pp. 137-141.

APPENDIX

Table 2. Operating conditions of the example turbines.

	Re (1V,exit)	Vane M_{exit}	Blade M_{exit}
HPT1	2.4×10^6	0.82	1.40
HPT2	2.1×10^6	1.09	1.24
HPT3	2.0×10^6	0.75	0.94
HPT4	2.0×10^6	0.61	0.81